

# FYX-051: A Novel and Potent Hybrid-Type Inhibitor of Xanthine Oxidoreductase

Koji Matsumoto, Ken Okamoto, Naoki Ashizawa, and Takeshi Nishino

Department of Biochemistry and Molecular Biology, Nippon Medical School, Tokyo, Japan (K.M., K.O., T.N.); and Research Laboratories 2, Fuji Yakuhin Co., Ltd., Saitama, Japan (K.M., N.A.)

Received September 8, 2010; accepted October 14, 2010

## ABSTRACT

4-[5-(Pyridin-4-yl)-1*H*-1,2,4-triazol-3-yl]pyridine-2-carbonitrile (FYX-051) is a potent inhibitor of bovine milk xanthine oxidoreductase (XOR). Steady-state kinetics study showed that it initially behaved as a competitive-type inhibitor with a  $K_i$  value of  $5.7 \times 10^{-9}$  M, then after a few minutes it formed a tight complex with XOR via a Mo-oxygen-carbon atom covalent linkage, as reported previously (*Proc Natl Acad Sci USA* **101**:7931-7936, 2004). Thus, FYX-051 is a hybrid-type inhibitor exhibiting both structure- and mechanism-based inhibition. The FYX-051-XOR complex decomposed with a half-life of 20.4 h, but the enzyme activity did not fully recover. This was found to be caused by XOR-mediated conversion of FYX-051 to 4-[5-(2-hydroxypyridin-4-yl)-1*H*-1,2,4-triazol-3-yl]pyridine-2-carbonitrile (2-hydroxy-FYX-051), as well as for-

mation of 6-hydroxy-4-[5-(2-hydroxypyridin-4-yl)-1*H*-1,2,4-triazol-3-yl]pyridine-2-carbonitrile (dihydroxy-FYX-051) and 4-[5-(2,6-dihydroxypyridin-4-yl)-1*H*-1,2,4-triazol-3-yl]-6-hydroxypyridine-2-carbonitrile (trihydroxy-FYX-051) during prolonged incubation for up to 72 h. A distinct charge-transfer band was observed concomitantly with the formation of the trihydroxy-FYX-051-XOR complex. Crystallographic analysis of the charge-transfer complex indicated that a Mo-nitrogen-carbon bond was formed between molybdenum of XOR and the nitrile group of trihydroxy-FYX-051. FYX-051 showed a potent and long-lasting hypouricemic effect in a rat model of potassium oxonate-induced hyperuricemia, and it seems to be a promising candidate for the clinical treatment of hyperuricemia.

## Introduction

Mammalian xanthine oxidoreductase (XOR) catalyzes the last two steps in the purine degradation pathway before formation of uric acid, i.e., hydroxylation of hypoxanthine to xanthine and xanthine to uric acid. The enzyme is a homodimer with molecular mass of 290 kDa; each subunit contains one molybdenum cofactor, two [2Fe-2S] centers, and one FAD center. The oxidative hydroxylation of purine substrates takes place at the molybdenum center, and reducing equivalents thus introduced are transferred via the two [2Fe-2S] centers to the FAD center, where reduction of the physiological electron acceptor, NAD<sup>+</sup> or O<sub>2</sub>, occurs. XOR is a good target of drugs to treat gout and hyperuricemia. Allopurinol [4-hydroxypyrazolo(3,4-*d*)pyrimidine] (Fig. 1C), a hy-

poxanthine isomer, was introduced by Elion et al. (1963) as an inhibitor of XOR more than 40 years ago and has been extensively prescribed for gout and hyperuricemia patients since then. Massey et al. (1970) reported that the hydroxylated metabolite produced by XOR, oxipurinol [4,6-dihydroxypyrazolo(3,4-*d*)pyrimidine], binds tightly to the reduced Mo(IV) of the enzyme. Crystal structure analysis of the oxipurinol-bound form of the reduced bovine XOR indicated that the water-exchangeable -OH ligand of the Mo(IV) atom was replaced by N2 of oxipurinol (Okamoto et al., 2008) (Fig. 1D). It is known, however, that oxipurinol dissociates with  $t_{1/2} = 300$  min at 25°C from the molybdenum, owing to spontaneous reoxidation of Mo(IV) to Mo(VI) (Massey et al., 1970). Therefore, despite the excellent pharmacokinetics properties of allopurinol, administration at a relatively high dose is normally required, and it can, although rarely, cause serious adverse effects such as fulminant hepatitis, renal failure, or Stevens-Johnson syndrome (Arellano and Sacristán, 1993). Many researchers have attempted to develop new inhibitors without these drawbacks. 2-(3-Cyano-4-isobutoxy-phenyl)-

This work was supported by the Ministry of Education, Science, Sport, and Culture of Japan [Grants 16205021, 20590317] and the National Project on Protein Structural and Functional Analyses.

Article, publication date, and citation information can be found at <http://jpet.aspetjournals.org>.  
doi:10.1124/jpet.110.174540.

**ABBREVIATIONS:** XOR, xanthine oxidoreductase; XO, xanthine oxidase; XDH, xanthine dehydrogenase; FYX-051, 4-[5-(pyridin-4-yl)-1*H*-1,2,4-triazol-3-yl]pyridine-2-carbonitrile; 2-hydroxy-FYX-051, 4-[5-(2-hydroxypyridin-4-yl)-1*H*-1,2,4-triazol-3-yl]pyridine-2-carbonitrile; trihydroxy-FYX-051, 4-[5-(2,6-dihydroxypyridin-4-yl)-1*H*-1,2,4-triazol-3-yl]-6-hydroxypyridine-2-carbonitrile; allopurinol, 4-hydroxypyrazolo(3,4-*d*)pyrimidine; oxipurinol, 4,6-dihydroxypyrazolo(3,4-*d*)pyrimidine; AFR, activity-to-flavin ratio; TEL-6720, 2-(3-cyano-4-isobutoxy-phenyl)-4-methyl-1,3-thiazole-5-carboxylic acid; Y-700, 1-[3-cyano-4-(2,2-dimethylpropoxy)phenyl]-1*H*-pyrazole-4-carboxylic acid; HPLC, high-pressure liquid chromatography; LC/MS, liquid chromatography/mass spectrometry.

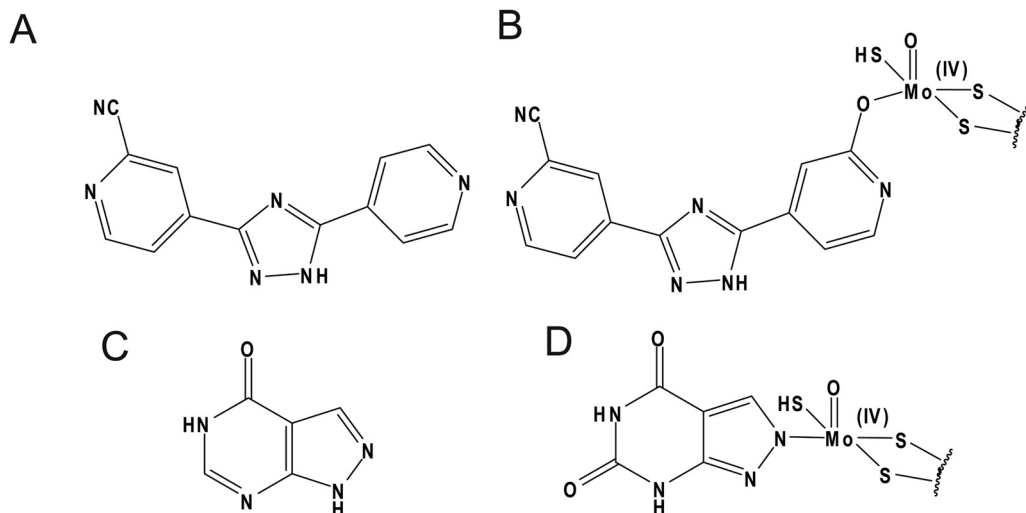


**Fig. 1.** Chemical structures of FYX-051 (A), allopurinol (C), and their hydroxylated forms bound to Mo(IV) (B and D).

4-methyl-1,3-thiazole-5-carboxylic acid (TEI-6720) (febuxostat) was developed as a nonpurine selective inhibitor of XOR, showing a more potent and longer-lasting urate-lowering effect than allopurinol in rodents (Osada et al., 1993) and chimpanzees (Komoriya et al., 1993). Clinical efficacy and tolerance to febuxostat have been confirmed (Becker et al., 2005), and the drug has been approved in both the United States and European Union for the treatment of gout.

4-[5-(Pyridin-4-yl)-1H-1,2,4-triazol-3-yl]pyridine-2-carbonitrile (FYX-051) (Fig. 1A) has been developed as another new type of XOR inhibitor. It not only forms a covalent linkage to molybdenum via oxygen in the hydroxylation reaction intermediate, but also interacts with amino acid residues of the solvent channel, such as the structure-based inhibitor TEI-6720 (Okamoto et al., 2003, 2004) or 1-[3-cyano-4-(2,2-dimethylpropoxy)phenyl]-1H-pyrazole-4-carboxylic acid (Y-700) (Fukunari et al., 2004) (Fig. 1B). In addition, because FYX-051 has high bioavailability and safety in animals (Shimo et al., 2005), it is a candidate drug for hyperuricemia and gout. Here, we investigated the inhibitor-enzyme interaction and the *in vivo* hypouricemic effect of FYX-051 to clarify the biochemical and pharmacological properties of this new inhibitor and its hydroxylated derivatives. We also report the prominent spectral perturbation of a trihydroxylated metabolite of the inhibitor, together with the results of crystallographic analysis of the enzyme-inhibitor complex.

## Materials and Methods

**Chemicals.** FYX-051 and 4-[5-(2-hydroxypyridin-4-yl)-1H-1,2,4-triazol-3-yl]pyridine-2-carbonitrile (2-hydroxy-FYX-051) were synthesized at Zieben Chemicals (Tokyo, Japan) and Fuji Yakuhin (Saitama, Japan), respectively. Allopurinol, oxipurinol, and potassium oxonate were purchased from Sigma-Aldrich (St. Louis, MO). All other reagents used were of the highest grade commercially available. For *in vitro* study, FYX-051 was dissolved in 0.1 N HCl. 2-Hydroxy-FYX-051, allopurinol, and oxipurinol were dissolved in 0.1 N NaOH. For *in vivo* study, FYX-051 and allopurinol were suspended in 0.5% (w/v) methylcellulose solution at a constant volume of 5 ml/kg body weight.

**Protein Purification.** Bovine milk xanthine oxidase (XO) was purified by using the method of Ball (1939). The active form of the enzyme was further separated from the inactive desulfo form by folate affinity chromatography according to the method of Nishino et al. (1981). The activity-to-flavin ratio (AFR) values of the prepared

enzyme, which were obtained by dividing the absorbance change per minute at 295 nm under standard assay conditions by the enzyme absorbance at 450 nm (Bray, 1975), were more than 180 (fully active enzyme has a value of 210) (Massey et al., 1970). The xanthine dehydrogenase (XDH) form of the enzyme was prepared according to the method of Eger et al. (2000). The concentration of the enzyme was determined spectrophotometrically by using a molar extinction of  $37,800 \text{ M}^{-1} \cdot \text{cm}^{-1}$  at 450 nm (Massey et al., 1969). The prepared enzyme was stored on ice without freezing in 20 mM pyrophosphate buffer, pH 8.5, 40 mM Tris-HCl buffer, pH 7.8, 1 mM salicylate, and 0.2 mM EDTA. Before use in experiments, the stored enzyme was subjected to gel filtration for removal of salicylate.

**Enzyme Assay.** Xanthine- $\text{O}_2$  activity was measured with a spectrophotometer (U-3200; Hitachi, Tokyo, Japan) at 295 nm by following the conversion of xanthine to uric acid. Assay mixture with various concentrations of xanthine and inhibitor in 0.1 M pyrophosphate buffer, pH 8.5 containing 0.2 mM EDTA was preincubated for several minutes, and reactions were started by adding XO to the mixture under the aerobic conditions at 25°C.

**Kinetic Study.** For the experiment on the time course of XO inhibition, the enzyme activity was measured by following the absorbance change for 1800 s in 3 ml of solution containing various concentrations of inhibitor, 0.15 mM xanthine, 0.1 M pyrophosphate buffer, pH 8.5, 0.2 mM EDTA, and 1 nM XO (AFR = 182). For the experiment on determination of  $K_i$  values, the enzyme activity was measured by following the absorbance change for 60 s in 3 ml of solution containing various concentrations of xanthine and inhibitor, 0.1 M pyrophosphate buffer, pH 8.5, 0.2 mM EDTA, and 5 or 10 nM XO (AFR = 186). Lineweaver-Burk plots of XO inhibition were made from reciprocal xanthine concentration, and absorbance change per minute was calculated from the change during the first few seconds of the initial phase.  $K_i$  and  $K_i'$  values were obtained from secondary plots of the slopes and  $1/V_{\text{max}}$  of the Lineweaver-Burk plots, respectively.

**Determination of Recovery Half-Lives of the Enzyme-Inhibitor Complexes.** Four-fifths equivalent of FYX-051 (5.1  $\mu\text{M}$ ) was first mixed anaerobically with 6.4  $\mu\text{M}$  XO (AFR = 189) in 1 ml of solution containing 20 mM pyrophosphate buffer, pH 8.5, 40 mM Tris-HCl buffer, pH 7.8, and 0.2 mM EDTA, and then the mixture was exposed to air. Aliquots were withdrawn for determination of urate formation activity at various incubation time points at 25°C under aerobic conditions. A 2-fold excess of 2-hydroxy-FYX-051 (32  $\mu\text{M}$ ) was also initially mixed with the enzyme (16  $\mu\text{M}$ ), then reduced with a 10-fold excess of hypoxanthine (320  $\mu\text{M}$ ) in 0.4 ml of the above buffer under anaerobic conditions. The mixture was incubated for 30 min at room temperature. Excess inhibitor and hypoxanthine were removed by gel filtration on a Sephadex G-25 column, then incuba-

tion was started at 25°C under aerobic conditions. Recovery half-lives of enzyme-inhibitor complexes were calculated from semilogarithmic plots of inhibition of urate formation.

**Determination of Metabolites by HPLC, LC/MS, and NMR.** Various concentrations of FYX-051 or allopurinol were mixed aerobically with 40  $\mu$ M XO (AFR = 189) in 1 ml of solution containing 20 mM pyrophosphate buffer, pH 8.5, 40 mM Tris-HCl buffer, pH 7.8, and 0.2 mM EDTA and the mixtures were incubated at 25°C under aerobic conditions. At various incubation time points, to eliminate proteins, five volumes of methanol was added to an aliquot of the enzyme-inhibitor complex solution, followed by centrifugation at 15,000 rpm for 10 min at 4°C. Twenty microliters of the supernatant was subjected to high-pressure liquid chromatography (HPLC; Alliance 2690 system/468 UV-VIS detector; Waters, Milford, MA) at 40°C on an Mightysil RP-18 GP column (Kanto Chemical, Tokyo, Japan). The mobile phase for the analysis of FYX-051 and its metabolites consisted of 0.5% acetic acid/acetonitrile (84:16), and that for allopurinol and oxipurinol consisted of 0.5% acetic acid at a flow rate of 1 ml/min. The UV absorbance was monitored at 300 nm for the former analysis and at 250 nm for the latter. Mass spectra of two unknown metabolites formed after prolonged incubation of the enzyme-FYX-051 complex were measured with a liquid chromatography/mass spectrometry (LC/MS) system (AP1150EX; Applied Biosystems, Foster City, CA) under the following operating conditions: column, Mightysil RP-18 GP; column temperature, 35°C; mobile phase, 0.5% acetic acid/acetonitrile (84:16); flow, 0.2 ml/min; injection volume, 5  $\mu$ l; ionization, positive mode electrospray. The metabolites were purified by solid-phase extraction with OASIS HLB cartridges (Waters) after sufficient amounts had been obtained by scaling up the enzyme-FYX-051 mixture volume. The chemical structure of one metabolite was assigned by NMR spectroscopy (JMN-EX270; JEOL, Tokyo, Japan). The other was used for the experiment on spectral changes of the enzyme-metabolite complex.

**Measurement of the Absorption Spectra of Enzyme-FYX-051 (or Metabolite) Complex.** For the preparation of the complex of the enzyme with FYX-051, four-fifths equivalent of FYX-051 (10  $\mu$ M) and fully active XO (13  $\mu$ M) were mixed anaerobically in 1 ml of solution containing 20 mM pyrophosphate buffer, pH 8.5, 40 mM Tris-HCl buffer, pH 7.8, and 0.2 mM EDTA. For the preparation of the complex of the enzyme with 4-[5-(2,6-dihydroxypyridin-4-yl)-1H-1,2,4-triazol-3-yl]-6-hydroxypyridine-2-carbonitrile (trihydroxy-FYX-051), equivalent amounts of purified trihydroxy-FYX-051 (11  $\mu$ M) and fully active XO (11  $\mu$ M) in 1 ml of the above buffer were mixed anaerobically, followed by reductive titration with sodium dithionite using a gas-tight titrating syringe. Spectral changes of both complexes after incubation at room temperature were measured with a spectrophotometer (DU-7400; Beckman Coulter, Fullerton, CA).

**Crystallization of XDH-FYX-051 (or Metabolite) Complex.** Crystals of the FYX-051 complex of bovine XDH were obtained by modification of a published method (Eger et al., 2000). To obtain the metabolite complex, salicylate was removed from enzyme stock solutions by gel filtration, and the sample was then diluted to a protein concentration of approximately 6 mg/ml. One and a half volumes of FYX-051 was mixed anaerobically with the enzyme, and the absorption spectrum of the mixture was monitored at room temperature until the charge transfer band approximately 600 nm reached the maximum. Then the enzyme-inhibitor mixture was transferred to an argon atmosphere, under which all subsequent manipulations were performed. The enzyme-inhibitor mixture was concentrated with a centrifugal filter unit (Microcon YM-100; Millipore Corporation, Billerica, MA) to a protein concentration of approximately 60 mg/ml, and then 30 mg/ml enzyme solution containing 30% (w/v) glycerol and 5 mM dithiothreitol was prepared. Aliquots (10  $\mu$ l) of enzyme solution were mixed with 10  $\mu$ l of 50 mM potassium phosphate buffer, pH 6.5, containing 8.0 to 9.5% polyethylene glycol 4000, 30% glycerol (w/v), 0.2 mM EDTA, and 5 mM dithiothreitol. The solutions were dropped on siliconized glass plates and kept in the dark at 22°C

TABLE 1

Data collection and refinement statistics

Space group	C2
Unit cell axes (Å), unit cell angle (degree)	$a = 168.9$ $b = 124.7$ $c = 146.2$ , $\beta = 91.04$
Resolution range (Å)	33.5–2.2
Number of unique reflections (used for $R_{\text{free}}$ calculation)	144,234 (7582)
$R_{\text{sym}}$ (%) <sup>a</sup>	7.9
Completeness (%)	95.2
$R_{\text{cryst}}$ (%) ( $R_{\text{free}}$ ) <sup>b</sup>	21.7 (28.0)
Rmsd bond length (Å)	0.011
Rmsd bond angles (degree)	1.4
Number of nonhydrogen atoms	22167
Ramachandran plot (%) <sup>c</sup>	90.4, 8.5, 0.5, 0.6

Rmsd, root mean square deviation.

<sup>a</sup>  $R_{\text{sym}} = \sum_{hkl} \sum_j |I_j - \langle I \rangle| / \sum_{hkl} \sum_j I_j$ , where  $I_j$  is the  $i$ th measurement and  $\langle I \rangle$  is the weighted mean of all measurements of  $I$ .

<sup>b</sup>  $R_{\text{cryst}} = \sum_{hkl} |F_{\text{obs}} - F_{\text{calc}}| / F_{\text{obs}}$ , where  $F_{\text{obs}}$  and  $F_{\text{calc}}$  are the observed and calculated structure factors, respectively, and the summation is over the reflections used for model refinement.  $R_{\text{free}}$  was the same as  $R_{\text{cryst}}$  for 5% of the data randomly omitted from the total data.

<sup>c</sup> Ramachandran statistics indicate the fraction of residues in the most favored, additionally allowed, generously allowed, and disallowed regions of the Ramachandran diagram, as defined by the program CCP4 (Collaborative Computational Project Number 4, 1994).

in the argon-filled box. Crystals grew after 5 days; they belonged to the same C2 space group as the original crystals, with almost the same unit cell parameters of  $a = 168.9$  Å,  $b = 124.7$  Å,  $c = 146.2$  Å, and  $\beta = 91.0^\circ$ . The crystals were collected with a nylon loop, shock-frozen, and stored in liquid nitrogen.

**Data Collection and Data Refinement.** A complete 2.2-Å diffraction data set was collected at the Photon Factory (Tsukuba, Japan), beamline NW12A at  $\lambda = 1.000$  Å (Table 1). Data were processed with the program package HKL2000. The structure (Protein Data Bank code 3AM9) was solved by molecular replacement by using the program MOLREP (Vagin and Teplyakov, 1997) with salicylate-bound XDH (Protein Data Bank code 1FO4) as a search model. The molecular model was built by using the program Coot (Emsley and Cowtan, 2004). Refinement was done following standard protocols of the program CCP4 version 6.1 (Collaborative Computational Project Number 4, 1994). Figure 7 was generated with the program Pymol.

**Animals.** Male Wistar/ST strain rats (7 weeks old; purchased from Japan SLC, Inc., Shizuoka, Japan) were kept in an air-conditioned room with a standard 12-h light/dark cycle. They were given standard chow and water ad libitum throughout the acclimatization and experimental periods.

**Measurement of Serum Urate in Rats Treated with Inhibitors.** FYX-051 or allopurinol was orally administered to rats, and blood was collected under ether anesthesia from the orbital sinus at 0.5, 1, 2, 6, and 12 h after drug administration. To maintain hyperuricemia during the experimental period, potassium oxonate (250 mg/kg s.c.; uricase inhibitor) was repeatedly injected at 4-h intervals. The blood was allowed to clot for 1 h at room temperature and then centrifuged. Serum urate level was measured by the phosphotungstic acid method (Henry et al., 1957). ED<sub>50</sub> values of inhibitors were calculated from the extent of decrease compared with the control by using the probit method.

**Statistical Analysis.** The mean and standard deviation of serum urate levels were calculated, and the difference between the control and treated groups was analyzed by Dunnett's test (at significance levels of 5 and 1%).

## Results

**Time-Dependent Inhibition of XO with Inhibitors and the Stability of XO-Inhibitor Complexes.** FYX-051 displayed time- and concentration-dependent inhibition of urate formation under air-saturated conditions (Fig. 2A).

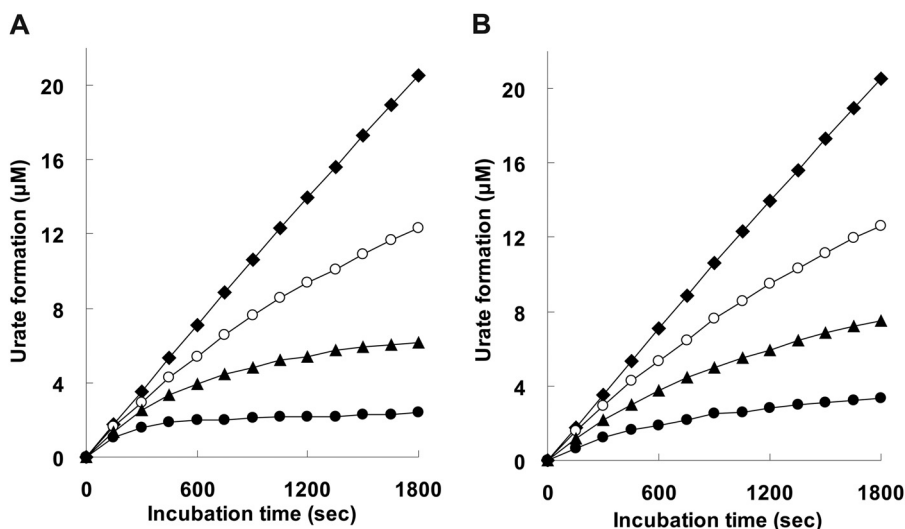


**Fig. 2.** Time-dependent inhibition of XO by FYX-051 (A) and 2-hydroxy-FYX-051 (B). Reactions were started by adding 1 nM XO (AFR = 182) to a solution of each inhibitor and 0.15 mM xanthine in 0.1 M pyrophosphate buffers, pH 8.5, containing 0.2 mM EDTA. The time course of xanthine- $O_2$  reactivity, expressed as urate formation, was observed photometrically by following the absorbance change at 295 nm, 25°C. A, FYX-051:  $\blacklozenge$ , no inhibitor, 0 nM;  $\circ$ , 3 nM;  $\blacktriangle$ , 10 nM;  $\bullet$ , 30 nM. B, 2-hydroxy-FYX-051:  $\blacklozenge$ , no inhibitor, 0 μM;  $\circ$ , 1 μM;  $\blacktriangle$ , 3 μM;  $\bullet$ , 10 μM.

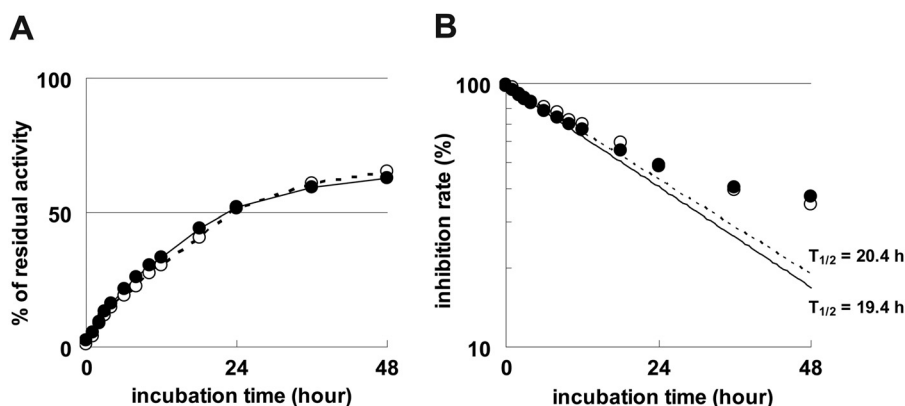


**Fig. 3.** Recovery of urate formation activity of XO-inhibitor complexes. A, FYX-051 (5.1 μM) was first mixed anaerobically with 6.4 μM XO (AFR = 189), and then the mixture was exposed to air. Aliquots were withdrawn for determination of urate formation at various incubation times at 25°C under aerobic conditions ( $\circ$ ). Excess 2-hydroxy-FYX-051 (32 μM) was also pre-mixed with hypoxanthine-reduced enzyme (16 μM) under anaerobic conditions, and incubation was started at 25°C after rapid removal of excess inhibitor and hypoxanthine by gel filtration at 4°C under aerobic conditions ( $\bullet$ ). B, semilogarithmic plots of A for determination of recovery half-lives.  $\circ$ , FYX-051;  $\bullet$ , 2-hydroxy-FYX-051.

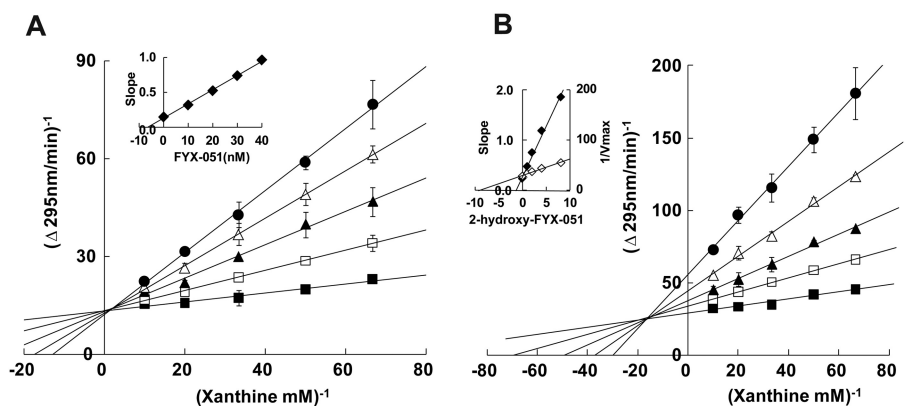


**Fig. 4.** Lineweaver-Burk plots of inhibition of XO by FYX-051 (A) and 2-hydroxy-FYX-051 (B). Reactions were started by adding 5 or 10 nM XO (AFR = 186) with various concentrations of inhibitor and xanthine in 0.1 M pyrophosphate buffer, pH 8.5, containing 0.2 mM EDTA. Activity was observed photometrically by following the absorbance change at 295 nm, 25°C. Initial velocities were used. Values are the means  $\pm$  S.D. of three experiments. A, FYX-051:  $\blacksquare$ , no inhibitor, 0 nM;  $\square$ , 10 nM;  $\blacktriangle$ , 20 nM;  $\triangle$ , 30 nM;  $\bullet$ , 40 nM. B, 2-hydroxy-FYX-051:  $\blacksquare$ , no inhibitor, 0 μM;  $\square$ , 1 μM;  $\blacktriangle$ , 2 μM;  $\triangle$ , 4 μM;  $\bullet$ , 8 μM. Inset, secondary plots of the Lineweaver-Burk plots. The  $K_i$  and  $K_i'$  values were obtained from the slopes ( $\blacklozenge$ ) and  $1/V_{max}$  ( $\diamond$ ), respectively.

2-Hydroxy-FYX-051, generated by primary hydroxylation of FYX-051 by XOR itself, also caused time- and concentration-dependent inhibition, although a relatively large amount of 2-hydroxy-FYX-051 was necessary to achieve potent inhibition (Fig. 2B) because of the lower affinity of 2-hydroxy-FYX-051, as determined from steady-state experiments (see below). We also estimated the stability of the XO-inhibitor complexes by determination of the recovery of enzyme activity (Fig. 3). The complexes of XO with inhibitors seem to be decomposed, probably caused by hydrolysis of the intermediate by water (Okamoto et al., 2004) under air-saturated conditions at 25°C, resulting in gradual recovery of the catalytic activity with a half-life ( $t_{1/2}$ ) of 20.4 h for the complex of

FYX-051 and 19.4 h for the complex of 2-hydroxy-FYX-051 (Fig. 3).

**Steady-State Analysis of Inhibition of XO.** Lineweaver-Burk plots of the enzyme inhibition by FYX-051 and 2-hydroxy-FYX-051 are shown in Fig. 4. FYX-051 exhibited competitive-type inhibition with a  $K_i$  value of  $5.7 \times 10^{-9}$  M by steady-state kinetics analyses based on initial velocity determination. In contrast, 2-hydroxy-FYX-051 showed mixed-type inhibition, but only weakly inhibited native XO ( $K_i = 1.5 \times 10^{-6}$  M,  $K_i' = 9.2 \times 10^{-6}$  M).

**Analysis of the Metabolites of FYX-051 Produced by XO.** The time course of metabolite production under air-saturated conditions at 25°C after mixing 36 μM FYX-051

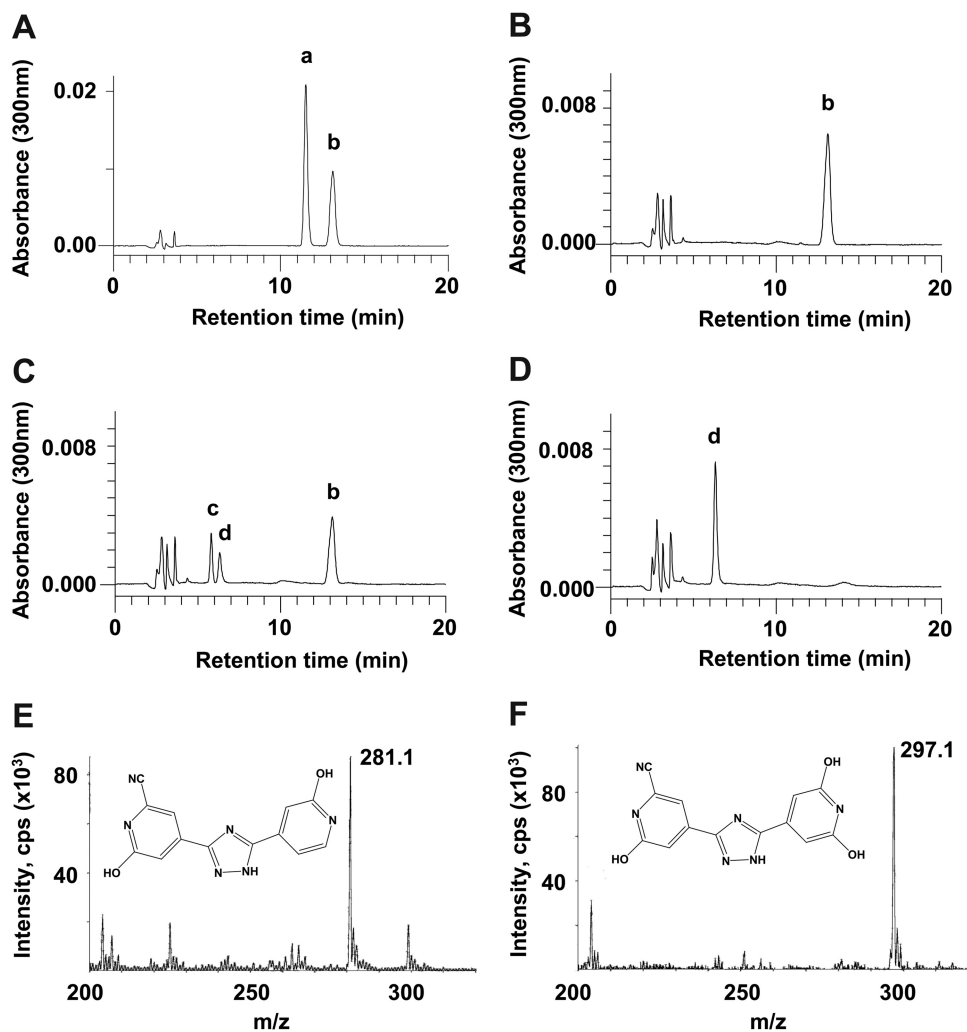


**Fig. 5.** Analysis of metabolites of FYX-051 produced by XO. FYX-051 (32  $\mu\text{M}$ ) was mixed aerobically with 40  $\mu\text{M}$  XO (AFR = 189), and the mixture was incubated at 25°C. Metabolites of FYX-051 were evaluated by HPLC and LC/MS. A, authentic standards of FYX-051 and 2-hydroxy-FYX-051. B, immediately after mixing. C, 8 h after mixing. D, 72 h after mixing. E, MS profile of peak c. F, MS profile of peak d.

with 40  $\mu\text{M}$  XO is shown in Fig. 5, A–D. All of the FYX-051 (peak a) was quickly converted to 2-hydroxy-FYX-051 (peak b) upon incubation with XO. Thereafter, 2-hydroxy-FYX-051 gradually decreased, and peaks of two other metabolites (peaks c and d) appeared within 8 h. Whereas peak c rapidly vanished, peak d was stable for at least 72 h. LC/MS analysis (Fig. 5, E and F) showed that peaks c and d had molecular masses of 280 and 296, i.e., 32 and 48 mass units larger than FYX-051, respectively. Peaks c and

d were purified by solid-phase extraction using OASIS HLB cartridges, and structure determination of the compound obtained from peak c was performed with NMR spectroscopy. It was found that the second and third hydroxylations occurred sequentially at the 6-position of the pyridinecarbonitrile ring (Fig. 5E) and the 6-position of the hydroxypyridine ring (Fig. 5F), respectively.

**Spectral Changes of XO on Mixing with FYX-051 and Trihydroxy-FYX-051.** As described previously (Okamoto et

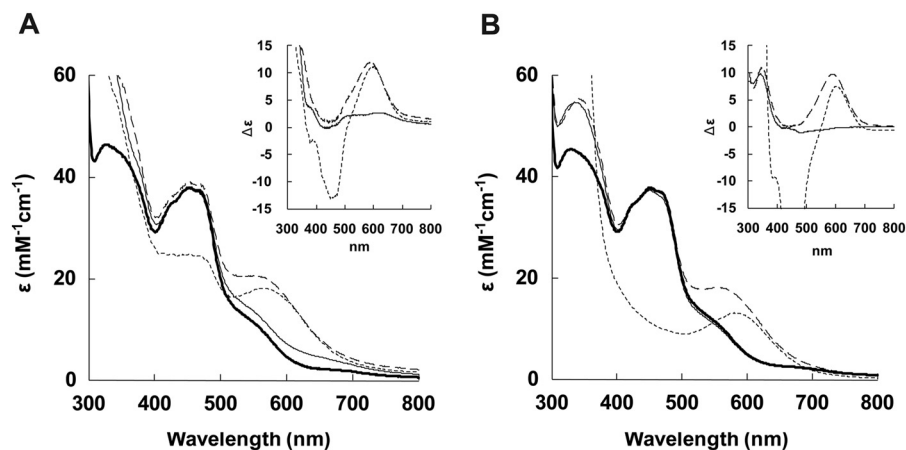


**Fig. 6.** A, the absorption spectra of XO after mixing with FYX-051 under anaerobic conditions. The spectrum of the enzyme before mixing with FYX-051 (bold solid line), immediately after (solid line), 120 h after (dotted line), and 30 min after exposure to air (dashed line) is shown. Inset, difference spectra between enzyme before and after mixing with FYX-051. B, the absorption spectra of XO after mixing with trihydroxy-FYX-051 under anaerobic conditions. The spectrum of the enzyme before mixing with trihydroxy-FYX-051 (bold solid line), immediately after (solid line), 10 min after dithionite reduction (dotted line), and 10 min after exposure to air (dashed line) is shown. Inset, difference spectra between enzyme before and after mixing with trihydroxy-FYX-051.

al., 2004), immediate spectral changes were observed on mixing XOR with FYX-051 because of formation of a covalent reaction intermediate (Fig. 6A). However, on prolonged incubation (120 h after mixing), further spectral changes were observed with the appearance of a larger positive peak at 600 nm and a negative peak at 450 nm. No further changes occurred on incubation for longer than 120 h. When air was admitted, the negative peak at 450 nm completely disappeared, but the larger positive peak at 590 nm ( $\Delta\epsilon = 11.9 \text{ mM}^{-1} \cdot \text{cm}^{-1}$ ) remained stable for at least 30 min. We also observed the spectral changes of dithionite-reduced XO with trihydroxy-FYX-051 (Fig. 6B) to confirm the nature of the spectral changes. An identical charge-transfer complex with a large positive peak at 590 nm ( $\Delta\epsilon = 9.7 \text{ mM}^{-1} \cdot \text{cm}^{-1}$ ) was obtained after reoxidation of the enzyme by exposure to air, indicating that reduced molybdenum and trihydroxy-FYX-051 form an identical complex with that shown in Fig. 6A.

**Crystal Structure of XDH-FYX-051-Metabolite Complex.** XOR was incubated with FYX-051 until marked spectral perturbation was observed (120 h), then the complex was crystallized. The crystals were collected and frozen anaerobically, and the crystal structure was determined at 2.2-Å resolution. In the xanthine-binding site, the metabolite is bound in the solvent channel associated with the xanthine hydroxylation site and is linked with molybdopterin (Fig. 7). Based on our analysis of the metabolites of FYX-051 produced by XO (Fig. 5), we constructed a model with trihydroxy-FYX-051 as the ligand. Trihydroxy-FYX-051 binds with its nitrile residue close to the molybdenum. From the electron density, covalent linkage of the molybdenum and the pyridine ring via oxygen that is to be incorporated into the hydroxyl residue seems unlikely. It seems more likely

that the pyridine ring is connected with molybdenum via the nitrile residue of the compound (Fig. 7).

**Conversion of FYX-051 and Allopurinol to Monohydroxylated Metabolites by XO.** Figure 8 compares the formation of monohydroxylated metabolites from FYX-051 and allopurinol by XO after aerobic incubation for 5 min at 25°C. When equimolar FYX-051 was mixed with 40  $\mu\text{M}$  XO, most of the FYX-051 in the mixture was immediately converted to 2-hydroxy-FYX-051, and the enzyme activity was completely inhibited. Even if a 3- or 10-fold molar excess of FYX-051 was mixed with the enzyme, the amount of 2-hydroxy-FYX-051 formed did not exceed that of the enzyme. In contrast, excess allopurinol was converted mostly to oxipurinol, regardless of the amount of the enzyme. A 30-fold molar excess of allopurinol was required for full inactivation of the enzyme.

**Hypouricemic Effect of FYX-051 in Oxonate-Induced Hyperuricemic Rats.** Changes in serum urate levels of rats at 1 h after oral administration of FYX-051 and allopurinol are shown in Fig. 9A. Serum urate levels in oxonate-injected rats were increased to 4 mg/dl or less and maintained at high levels by repeated oxonate injection throughout the experimental period. In this hyperuricemic model, FYX-051 in the dose range of 0.03 to 1 mg/kg caused a dose-dependent decrease in serum urate levels with an extremely low  $\text{ED}_{50}$  of 0.15 mg/kg, evaluated at 1 h after oral administration. Allopurinol in the dose range of 1 to 30 mg/kg also displayed dose dependence, but had a relatively high  $\text{ED}_{50}$  value of 4.7 mg/kg. Figure 9B shows the time course of changes in the  $\text{ED}_{50}$  values of FYX-051 and allopurinol in this model. FYX-051 was very effective even long after administration, and its  $\text{ED}_{50}$  values at 6 and 12 h were 0.25 and 0.70 mg/kg, respectively. On the other hand, allopurinol was less potent, and

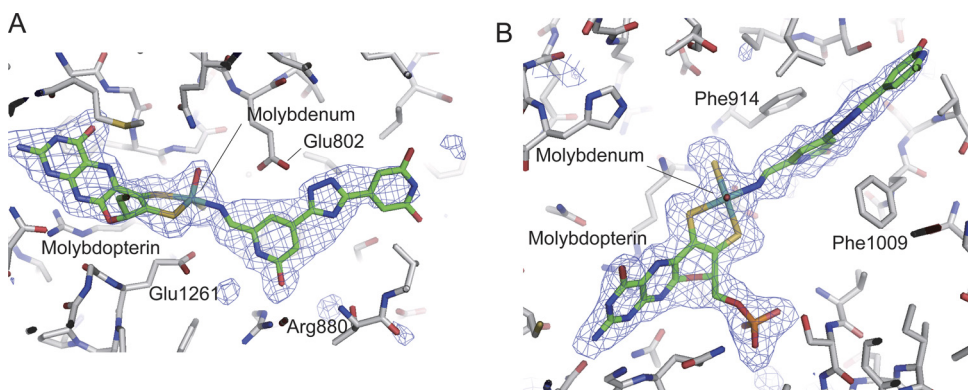


**Fig. 7.** Crystal structure of XOR after 5 days of incubation with FYX-051.  $F_o - F_c$  electron density of two different angle views (A and B) corresponding to molybdopterin-hydroxylated derivative of FYX-051, contoured at a  $3.0\text{-}\sigma$  cutoff. The  $F_o - F_c$  density was calculated before introducing the molybdopterin and hydroxylated FYX-051 into the crystallographic model to avoid model bias. Carbon atoms of molybdopterin-hydroxylated FYX-051 are illustrated in green. Some amino acid residues important for catalysis and substrate binding are labeled.

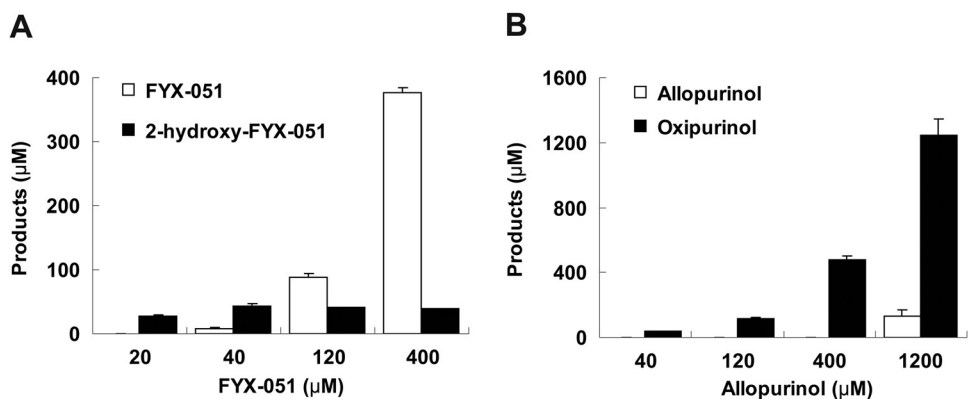


**Fig. 8.** Conversion of FYX-051 (A) and allopurinol (B) to monohydroxylated metabolites by XO. Various concentrations of FYX-051 and allopurinol were mixed aerobically with 40  $\mu\text{M}$  XO. Unchanged forms and monohydroxylated metabolites (2-hydroxy-FYX-051 and oxipurinol) in the mixtures were quantified by HPLC after 5-min incubation at 25°C. Values are the means  $\pm$  S.D. of three experiments.

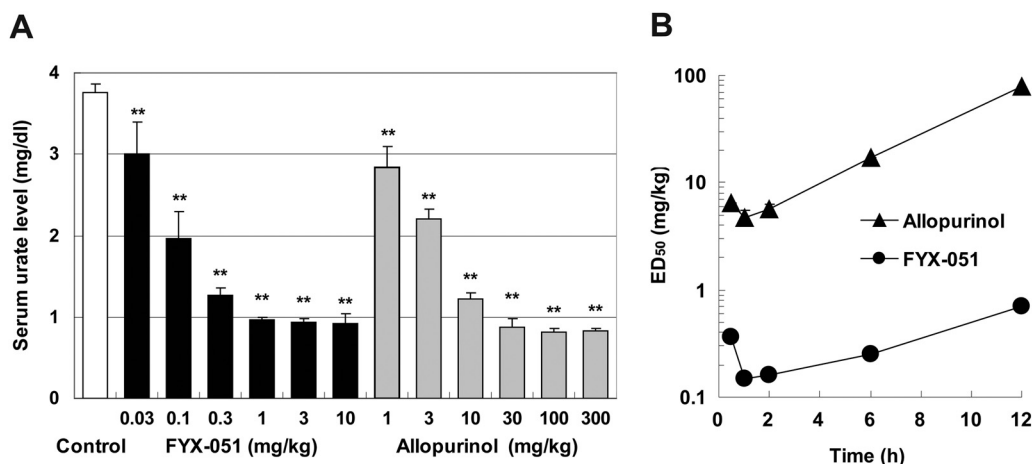


**Fig. 9.** Hypouricemic effects of FYX-051 and allopurinol in oxonate-induced hyperuricemic rats. A, changes in serum urate levels of hyperuricemic rats at 1 h after oral administration of FYX-051 or allopurinol. \*\*,  $p < 0.01$  versus control group (Dunnett's multiple range test). B, time course of changes in the ED<sub>50</sub> values of FYX-051 and allopurinol in this model. Values are the means  $\pm$  S.D. ( $n = 5$ ).

the ED<sub>50</sub> values at 6 and 12 h after administration were 17 and 78 mg/kg, respectively.

## Discussion

In the time course study of XOR inhibition, we found that FYX-051 displayed time-dependent inhibition to urate formation (Fig. 2). Okamoto et al. (2004) showed that such time-dependent inhibition is caused by formation of a stable reaction intermediate by determination of the crystal structure of the FYX-051-XDH complex. This showed that FYX-051 forms a covalent bond to molybdenum via oxygen, i.e., a Mo-O-C2-FYX-051 bond. It seems likely that 2-hydroxy-FYX-051, which also exhibits time-dependent inhibition, would interact similarly with XOR, that is, it would undergo further hydroxylation by the enzyme to form another stable reaction intermediate.

The study of complex stability (Fig. 3) by determination of the recovery of enzyme activity showed that the FYX-051-XOR complex (Fig. 1B) decomposed with a half-life of 20.4 h, which was more stable than the oxipurinol XOR complex (Fig. 1D) with 5 h (Massey et al., 1970). It is noteworthy that the recovery of enzyme activity from the FYX-051-XOR complex gradually slowed down, and full enzyme activity was not recovered for 48 h, which is consistent with the indication from the time-dependent inhibition studies that 2-hydroxy-FYX-051 and/or a further hydroxylated form of 2-hydroxy-FYX-051 might also have an inhibitory effect.

Although FYX-051 showed potent, time-dependent inhibition of XOR caused by the formation of stable reaction intermediates, as described above, FYX-051 and its derivative also display structure-based noncovalent inhibition, as shown by steady-state kinetic analyses based on initial velocity determination (Fig. 4). FYX-051 exhibited competitive-type inhibition with a  $K_i$  value of  $5.7 \times 10^{-9}$  M, two orders of magnitude smaller than that of allopurinol found by means of steady-state analysis ( $K_i = 7.0 \times 10^{-7}$  M) (Elion, 1966). Previous study of the crystal structure revealed that the FYX-051-XDH complex has various interactions involving amino acid residues in the substrate channel of the enzyme, in addition to the covalent bond to molybdenum (Okamoto et al., 2004). Accordingly, the potent inhibition of the enzyme by FYX-051 in the initial phase can be ascribed to such structural interactions.

Analysis of the metabolites of FYX-051 produced by XOR showed that 2-hydroxy-FYX-051, a monohydroxylated metabolite of FYX-051, was further converted to dihydroxy- and trihydroxy-FYX-051 during prolonged incubation for up to 72 h (Fig. 5). These structures are reasonable in terms of the nature of XOR, which normally hydroxylates the carbon atom adjacent to the nitrogen atom of a heterocycle (Okamoto et al., 2004). Trihydroxy-FYX-051 was stable for at least 72 h, so that this trihydroxy compound may mediate mainly the inhibition and be responsible for the spectral perturbation of XO (Figs. 3 and 6).

On prolonged incubation of the FYX-051-XOR complex, further spectral changes were observed with the appearance of a larger positive peak at 590 nm (Fig. 6), suggesting the formation of a new stable charge-transfer complex between the reduced molybdenum center and a metabolite of FYX-051. This is confirmed by the fact that the identical spectrum of the charge-transfer complex was obtained from the trihydroxy-FYX-051-XOR complex. The wavelength of maximum absorption ( $\lambda_{\max} = 590$  nm) of these charge-transfer complexes was shifted 50 nm to shorter wavelength than that in the case of 2-hydroxy-FYX-051 ( $\lambda_{\max} = 640$  nm) (Okamoto et al., 2004), the violapterin complex (Davis et al., 1982), or the complexes with oxipurinol and its derivatives (Massey et al., 1970). Thus, the complex of XDH-trihydroxy-FYX-051 is suggested to be quite different from the complexes of XDH with 2-hydroxy-FYX-051 or pyrazolo pyrimidine derivatives. The crystal structure of the FYX-051-XOR complex with marked spectral perturbation reveals that the pyridine ring of trihydroxy-FYX-051 is connected with molybdenum via the nitrile residue of the compound (Fig. 7). The distance between the molybdenum and C1 carbon atom of the ring is 4.3 Å, which is clearly larger than that of the complex with FYX-051 (Okamoto et al., 2004) and fits well with a linkage via the nitrile group. This finding suggests that trihydroxy-FYX-051 forms a covalently bound complex with the molybdenum that is quite different from the reaction intermediate structure (Okamoto et al., 2004). The 2,6-dihydroxypyridine ring binds at the outermost region of the channel and is not clearly defined. The crystal structure of the trihydroxy-FYX-051-bound form is basically different from that of the FYX-051-bound form, indicating that a major reason for the spectral change is a direct influence of the different covalent linkages between the inhibitor and the molybdenum cofactor. We sug-

gest that the nitrile group would markedly perturb the electronic environment of the molybdopterine cofactor.

In previous *in vivo* study, allopurinol is immediately converted to oxipurinol, which is detected in human plasma and urine at relatively high concentration (Hosoya et al., 1991), whereas only a little 2-hydroxy-FYX-051 is detected in human urine after the administration of FYX-051 (Nakazawa et al., 2006). In the present study, we investigated *in vitro* hydroxylation by XO to clarify the difference in metabolic behavior between two inhibitors *in vivo*. These results imply that 2-hydroxy-FYX-051 enzyme complex is so stable (Fig. 3;  $t_{1/2}$  = approximately 20 h) that only a little 2-hydroxy-FYX-051 can be dissociated from the complex (Fig. 8). Furthermore, 2-hydroxy-FYX-051 was slightly increased when incubation was continued, and no formation of metabolites with two or three hydroxyl groups was observed until nonreacted FYX-051 was completely consumed (data not shown). It is likely that this reflects the difference in binding affinity between FYX-051 and 2-hydroxy-FYX-051 for the enzyme. It is likely that the conversion of allopurinol to oxipurinol continues until the oxipurinol-enzyme complex is fully formed, because allopurinol is a good substrate for XOR. This oxipurinol, which is deposited in the kidney during renal excretion, sometimes causes severe adverse effects in patients with renal insufficiency (Hande et al., 1984). In the case of FYX-051, such an adverse effect would not be expected, because 2-hydroxy-FYX-051 does not easily accumulate and is not renally excreted.

A previous study showed that repeated allopurinol dosing (30 mg/kg p.o. once daily for 28 days) in normal rats caused severe nephrotoxicity (Horiuchi et al., 1999). On the other hand, we previously demonstrated that nephropathy in rats occurring after FYX-051 dosing (1 mg/kg p.o. once daily for 28 days) was a secondary change caused by xanthine crystals being deposited in the kidney because of the potent inhibition of XOR (Shimo et al., 2005). Accordingly, it is likely that the potent and long-lasting hypouricemic effects of FYX-051 (Fig. 9) arise from its high affinity for the enzyme and stable binding to the enzyme.

In conclusion, we have studied in detail how FYX-051 interacts with bovine milk XOR. It was found that the 2-hydroxy-FYX-051-XOR complex formed is more stable than the oxipurinol-XOR complex, although FYX-051, as well as allopurinol, forms a covalent linkage to molybdenum (Okamoto et al., 2004) and exhibits time-dependent inhibition of the enzyme. FYX-051 also displayed a potent, noncovalent inhibition of XOR with a lower  $K_i$  value of  $5.7 \times 10^{-9}$  M than allopurinol. Moreover, we found that XOR hydroxylates three carbons of FYX-051 and finally generates a trihydroxylated derivative, which forms a covalent linkage to molybdenum via the nitrile group and brings a distinct spectral change of the enzyme. However, only a little 2-hydroxy-FYX-051 was detected, and no other hydroxylation metabolites were observed in an *in vivo* study (Nakazawa et al., 2006). Dihydroxylated and trihydroxylated forms of FYX-051 appeared only when the enzyme-inhibitor complex was incubated under artificial conditions, that is, under the condition of excess enzyme. Therefore, the pharmacological effects of the dihydroxylated and trihydroxylated metabolites should have no impact in the clinical context. Moreover, we have demonstrated that FYX-051 exerts a potent and long-lasting hypouricemic effect *in vivo*. These

effects of FYX-051 may arise from its high affinity for XOR and stable binding to XOR *in vitro*. Therefore, FYX-051 appears to be a promising candidate drug for the treatment of gout and hyperuricemia.

#### Acknowledgments

We thank Drs. Tomohiro Matsumura and Teruo Kusano (Nippon Medical School, Tokyo, Japan) for data collection of crystallographic data; Mr. Koichi Omura and Dr. Takahiro Sato (Fuji Yakuhin, Saitama, Japan) for LC/MS and NMR analyses; officials at the Photon Factory (Tsukuba, Japan) for beam time; and the beam line staff of NW12A for support.

#### Authorship Contributions

*Participated in research design:* Matsumoto, Okamoto, Ashizawa, and Nishino.

*Conducted experiments:* Matsumoto, Okamoto, and Ashizawa.

*Contributed new reagents or analytic tools:* Matsumoto and Ashizawa.

*Performed data analysis:* Matsumoto, Okamoto, and Nishino.

*Wrote or contributed to the writing of the manuscript:* Matsumoto, Okamoto, and Nishino.

*Other:* Nishino acquired funding for the research.

#### References

- Arellano F and Sacristán JA (1993) Allopurinol hypersensitivity syndrome: a review. *Ann Pharmacother* **27**:337–343.
- Ball EG (1939) Xanthine oxidase: purification and properties. *J Biol Chem* **128**: 51–67.
- Becker MA, Schumacher HR Jr, Wortmann RL, MacDonald PA, Eustace D, Palo WA, Streit J, and Joseph-Ridge N (2005) Febuxostat compared with allopurinol in patients with hyperuricemia and gout. *N Engl J Med* **353**:2450–2461.
- Bray RC (1975) Molybdenum iron-sulfur flavin hydroxylases and related enzymes, in *The Enzymes* (Boyer PD ed) vol VII, part B, pp 299–419, Academic Press, New York.
- Collaborative Computational Project Number 4 (1994) The CCP4 suite: programs for protein crystallography. *Acta Crystallogr D Biol Crystallogr* **50**:760–763.
- Davis MD, Olson JS, and Palmer G (1982) Charge transfer complexes between pteridine substrates and the active center molybdenum of xanthine oxidase. *J Biol Chem* **257**:14730–14737.
- Eger BT, Okamoto K, Enroth C, Sato M, Nishino T, Pai EF, and Nishino T (2000) Purification, crystallization and preliminary X-ray diffraction studies of xanthine dehydrogenase and xanthine oxidase isolated from bovine milk. *Acta Crystallogr D Biol Crystallogr* **56**:1656–1658.
- Eliion GB (1966) Enzymatic and metabolic studies with allopurinol. *Ann Rheum Dis* **25**:608–614.
- Eliion GB, Callahan S, Nathan H, Bieber S, Rundles RW, and Hitchings GH (1963) Potentiation by inhibition of drug degradation: 6-substituted purines and xanthine oxidase. *Biochem Pharmacol* **12**:85–93.
- Emsley P and Cowtan K (2004) Coot: model-building tools for molecular graphics. *Acta Crystallogr D Biol Crystallogr* **60**:2126–2132.
- Fukunari A, Okamoto K, Nishino T, Eger BT, Pai EF, Kamezawa M, Yamada I, and Kato N (2004) Y-700[1-[3-cyano-4-(2,2-dimethylpropoxy)phenyl]-1H-pyrazole-4-carboxylic acid]: a potent xanthine oxidoreductase inhibitor with hepatic excretion. *J Pharmacol Exp Ther* **311**:519–528.
- Hande KR, Noone RM, and Stone WJ (1984) Severe allopurinol toxicity. Description and guidelines for prevention in patients with renal insufficiency. *Am J Med* **76**:47–56.
- Henry RJ, Sobel C, and Kim J (1957) A modified carbonate-phosphotungstate method for the determination of uric acid and comparison with the spectrophotometric uricase method. *Am J Clin Pathol* **28**:152–160.
- Horiuchi H, Ota M, Kobayashi M, Kaneko H, Kasahara Y, Nishimura S, Kondo S, and Komoriya K (1999) A comparative study on the hypouricemic activity and potency in renal xanthine calculus formation of two xanthine oxidase/xanthine dehydrogenase inhibitors: TEL-6720 and allopurinol in rats. *Res Commun Mol Pathol Pharmacol* **104**:307–319.
- Hosoya T, Ichida K, Tabé A, and Sakai O (1991) A study on treatment of hyperuricemia—effects and kinetics of allopurinol and oxipurinol. *Ryumachi* **31**:28–35.
- Komoriya K, Osada Y, Hasegawa M, Horiuchi H, Kondo S, Couch RC, and Griffin TB (1993) Hypouricemic effect of allopurinol and the novel xanthine oxidase inhibitor TEL-6720 in chimpanzees. *Eur J Pharmacol* **250**:455–460.
- Massey V, Brumby PE, and Komai H (1969) Studies on milk xanthine oxidase: some spectral and kinetics properties. *J Biol Chem* **244**:1682–1691.
- Massey V, Komai H, Palmer G, and Eliion GB (1970) On the mechanism of inactivation of xanthine oxidase by allopurinol and other pyrazolo[3,4-d]pyrimidines. *J Biol Chem* **245**:2837–2844.
- Nakazawa T, Miyata K, Omura K, Iwanaga T, and Nagata O (2006) Metabolic profile of FYX-051 (4-(5-pyridin-4-yl-1h-[1,2,4]triazol-3-yl)pyridine-2-carbonitrile) in the rat, dog, monkey, and human: identification of N-glucuronides and N-glucosides. *Drug Metab Dispos* **34**:1880–1886.

- Nishino T, Nishino T, and Tsushima K (1981) Purification of highly active milk xanthine oxidase by affinity chromatography on Sepharose 4B/folate gel. *FEBS Lett* **131**:369–372.
- Okamoto K, Eger BT, Nishino T, Kondo S, Pai EF, and Nishino T (2003) An extremely potent inhibitor of xanthine oxidoreductase: crystal structure of the enzyme-inhibitor complex and mechanism of inhibition. *J Biol Chem* **278**:1848–1855.
- Okamoto K, Eger BT, Nishino T, Pai EF, and Nishino T (2008) Mechanism of inhibition of xanthine oxidoreductase by allopurinol: crystal structure of reduced bovine milk xanthine oxidoreductase bound with oxipurinol. *Nucleosides Nucleotides Nucleic Acids* **27**:888–893.
- Okamoto K, Matsumoto K, Hille R, Eger BT, Pai EF, and Nishino T (2004) The crystal structure of xanthine oxidoreductase during catalysis: implications for reaction mechanism and enzyme inhibition. *Proc Natl Acad Sci USA* **101**:7931–7936.
- Osada Y, Tsuchimoto M, Fukushima H, Takahashi K, Kondo S, Hasegawa M, and Komoriya K (1993) Hypouricemic effect of the novel xanthine oxidase inhibitor, TEI-6720, in rodents. *Eur J Pharmacol* **241**:183–188.
- Shimo T, Ashizawa N, Matsumoto K, Nakazawa T, and Nagata O (2005) Simultaneous treatment with citrate prevents nephropathy induced by FYX-051, a xanthine oxidoreductase inhibitor, in rats. *Toxicol Sci* **87**:267–276.
- Vagin A and Teplyakov A (1997) MOLREP: an automated program for molecular replacement. *J Appl Cryst* **30**:1022–1025.

---

**Address correspondence to:** Takeshi Nishino, Department of Biochemistry and Molecular Biology, Nippon Medical School, 1-1-5 Sendagi, Bunkyo-ku, Tokyo 113-8602, Japan. E-mail: nishino@nms.ac.jp

---